

Clouds damp the radiative impacts of Polar sea ice loss

Authors: Ramdane Alkama^{1*}, Alessandro Cescatti¹, Patrick C. Taylor^{2*}, Lorea Garcia-San Martin¹, Herve Douville³, Gregory Duveiller¹, Giovanni Forzieri¹ and Didier Swingedouw⁴

Affiliation:

¹ European Commission, Joint Research Centre, Via E. Fermi, 2749, I-21027 Ispra (VA), Italy

² NASA Langley Research Center, Hampton, Virginia

³ Centre National de Recherches Meteorologiques, Meteo-France/CNRS, Toulouse, France

⁴ EPOC, Universite Bordeaux 1, Allée Geoffroy Saint-Hilaire, Pessac 33615, France

***Correspondence to:** Ramdane Alkama (ram.alkama@hotmail.fr)

Patrick C. Taylor (patrick.c.taylor@nasa.gov)

Abstract

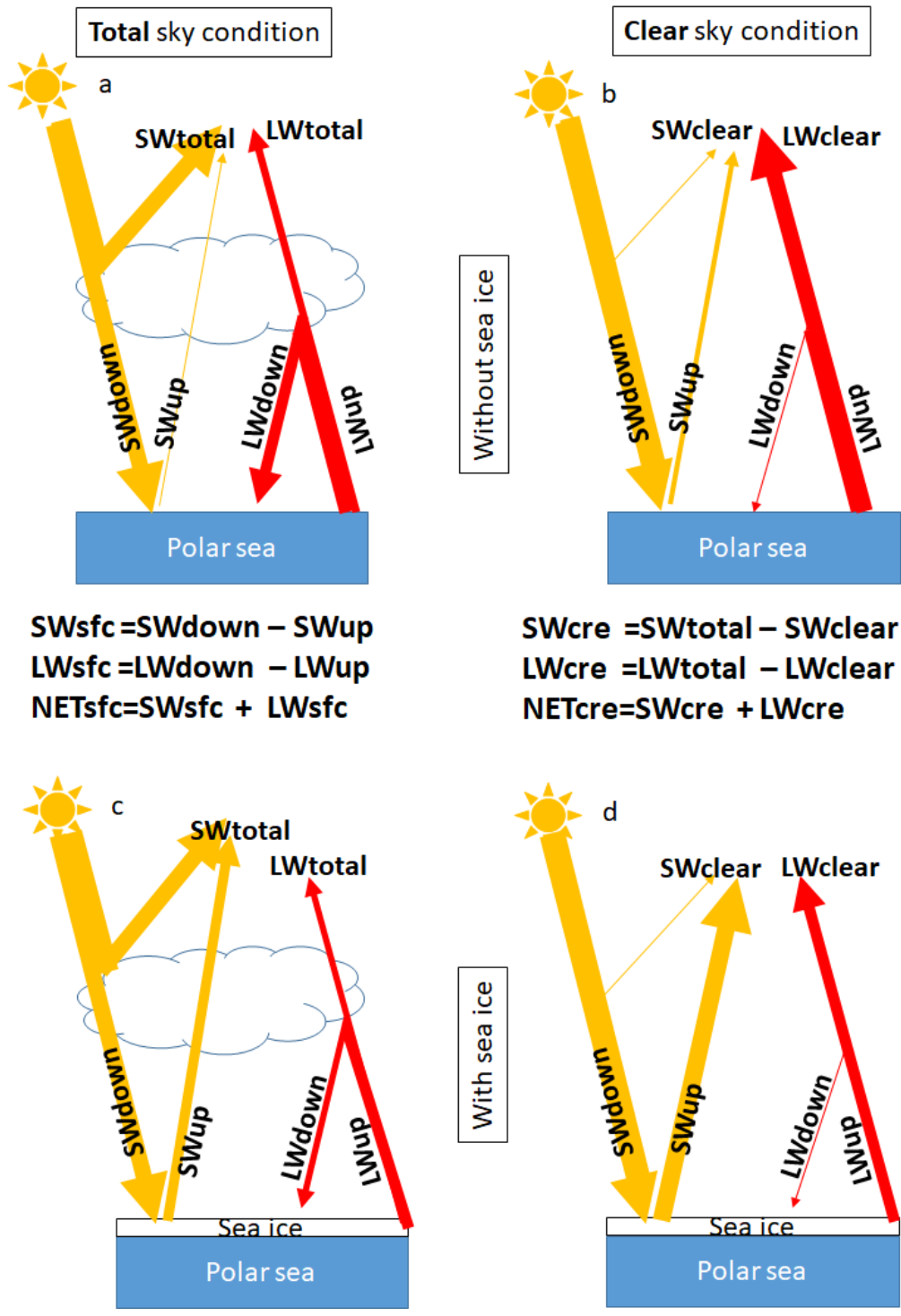
Clouds play an important role in the climate system: (1) cooling the Earth by reflecting incoming sunlight to space and (2) warming the Earth by reducing thermal energy loss to space. Cloud radiative effects are especially important in polar regions and have the potential to significantly alter the impact of sea ice decline on the surface radiation budget. Using CERES data and 32 CMIP5 climate models, we quantify the influence of polar clouds on the radiative impact of polar sea ice variability. Our results show that the cloud shortwave cooling effect strongly influences the impact of sea ice variability on the surface radiation budget and does so in a counter-intuitive manner over the polar seas: years with less sea ice and a larger net surface radiative flux show a more negative cloud radiative effect. Our results indicate that $66 \pm 2\%$ of this change in the net cloud radiative effect is due to the reduction in surface albedo and the remaining $34 \pm 1\%$ is due to an increase in cloud cover/optical thickness. The overall cloud radiative damping effect is $56 \pm 2\%$ over the Antarctic and $47 \pm 3\%$ over the Arctic. Thus, present-day cloud properties significantly reduce the net radiative impact of sea ice loss on the Arctic and Antarctic surface radiation budgets. As a result, climate models must accurately represent present-day polar cloud properties in order to capture the surface radiation budget impact of polar sea ice loss and thus the surface albedo feedback.

37 1. Introduction

38 Solar radiation is the primary energy source for the Earth system and provides the energy driving
39 motions in the atmosphere and ocean, the energy behind water phase changes, and for the energy
40 stored in fossil fuels. Only a fraction (Loeb et al., 2018) of the solar energy arriving to the top of
41 the Earth atmosphere (shortwave radiation, SW) is absorbed at the surface. Some of it is reflected
42 back to space by clouds and by the surface, while some is absorbed by the atmosphere. In parallel,
43 the Earth's surface and atmosphere emit thermal energy back to space, called outgoing longwave
44 (LW) radiation, resulting in a loss of energy (Fig. 1). The balance between these energy exchanges
45 determines Earth's present and future climate. The change in this balance is particularly important
46 over the Arctic where summer sea ice is retreating at an accelerated rate (Comiso et al., 2008),
47 surface albedo is rapidly declining, and surface temperatures are rising at a rate double that of the
48 global average (Cohen et al., 2014; Graversen et al., 2008), impacting sub-polar ecosystems
49 (Cheung et al., 2009; Post et al., 2013) and possibly mid-latitude climate (Cohen et al., 2014;
50 Cohen et al. 2019).

51 Clouds play an important role in modifying the radiative energy flows that determine Earth's
52 climate. This is done both by increasing the amount of SW reflected back to space and by reducing
53 the LW energy loss to space relative to clear skies (Fig. 1). These cloud effects on Earth's radiation
54 budget can be gauged using the Cloud Radiative Effect (CRE), defined as the difference between
55 the actual atmosphere and the same atmosphere without clouds (Charlock and Ramanathan, 1985).
56 The different spectral components of this effect can be estimated from satellite observations: the
57 global average SW cloud radiative effect (SWcre) is negative since clouds reflect incoming solar
58 radiation back to space resulting in a cooling effect. On the other hand, the LW cloud radiative
59 effect (LWcre) is positive since clouds reduce the outgoing LW radiation to space generating a
60 warming effect (Harrison et al., 1990; Loeb et al., 2018; Ramanathan et al., 1989).

61 Cloud properties and their radiative effects exhibits significant uncertainty in the polar regions
62 (e.g., Curry et al. 1996; Kay and Gettelman 2009; Boeke and Taylor 2016; Kato et al. 2018). For
63 instance, climate models struggle to accurately simulate cloud cover, optical depth, and cloud
64 phase (Cesana et al., 2012; Komurcu et al., 2014; Kay et al. 2016). An accurate representation of
65 polar clouds is necessary because they strongly modulate radiative energy fluxes at the surface, in
66 the atmosphere, and at the TOA influencing the evolution of the polar climate systems. In addition,
67 polar cloud properties interact with other properties of the polar climate systems (e.g., sea ice) and
68 influence how variability in these properties affects the surface energy budget (Qu and Hall 2006;
69 Kay and L'Ecuyer 2013; Sledd and L'Ecuyer 2019). Moreover, Loeb et al. (2019) documented
70 severe limitations in the representation of surface albedo variations and their impact on the
71 observed radiation budget variability in reanalysis products, motivating the evaluation of radiation
72 budget variability over the polar seas in climate models. In this study, we use the Clouds and the
73 Earth's Radiant Energy System (CERES) top-of-atmosphere (TOA) and surface (SFC) radiative
74 flux datasets and 32 Coupled Model Intercomparison Project (CMIP5) climate models to estimate
75 the relationship between the CRE and the surface radiation budget in polar regions to improve our
76 understanding of how clouds modulate the surface radiation budget.



77

78

79 **Figure 1** Schematic representation of radiative energy flows in the polar seas under total sky
 80 conditions (a, c) and clear sky conditions (b, d) for two contrasting surface conditions: without sea
 81 ice (a, b) and with sea ice (c, d). All fluxes are taken positive downwards.

82

83 2. Methods and data

84 **2.1 CERES EBAF Ed4.0 Products:** Surface and TOA radiative flux quantities are taken from the
85 NASA CERES Energy Balanced and Filled (EBAF) monthly data set (CERES EBAF-TOA_Ed4.0
86 and CERES EBAF-SFC_Ed4.0), providing monthly, global fluxes on a $1^\circ \times 1^\circ$ latitude-longitude
87 grid (Loeb et al., 2018; Kato et al. 2018). CERES surface LW and SW radiative fluxes are used to
88 investigate the effect of clouds on the surface radiation budget response to sea ice variability over
89 the polar seas. CERES SFC EBAF radiative fluxes have been evaluated through comparisons with
90 46 buoys and 36 land sites across the globe, including the available high-quality sites in the Arctic.
91 Uncertainty estimates for individual surface radiative flux terms in the polar regions range from
92 12-16 $W m^{-2}$ (1σ) at the monthly mean $1^\circ \times 1^\circ$ gridded scale (Kato et al. 2018). CERES EBAF-
93 TOA and SFC radiative fluxes show a much higher reliability than other sources (e.g.,
94 meteorological reanalysis) and represent a key benchmark for evaluating the Arctic surface
95 radiation budget (Christensen et al. 2016; Loeb et al. 2019; Duncan et al. 2020).

96 In addition to radiative fluxes, cloud cover fraction (CCF) and cloud optical depth (COD) data
97 available from CERES EBAF data are used. Monthly mean CCF and COD data are derived from
98 instantaneous cloud retrievals using the Moderate-resolution Imaging Spectroradiometer
99 (MODIS) radiances (Trepte et al. 2019). Instantaneous retrievals are then spatially and
100 temporally averaged onto the $1^\circ \times 1^\circ$ monthly mean grid consistent with CERES EBAF.

101

102 **2.2 Cloud Radiative Effect:** CRE is used as a metric to assess the radiative impact of clouds on
103 the climate system, defined as the difference in net irradiance at TOA between total-sky and clear-
104 sky conditions. Using the CERES Energy Balanced And Filled (EBAF) Ed4.0 (Loeb et al., 2018)
105 flux measurements and CMIP5 simulated fluxes, CRE is calculated by taking the difference
106 between clear-sky and total-sky net irradiance flux at the TOA. All fluxes are taken as positive
107 downwards.

$$108 \quad SW_{cre} = SW_{total} - SW_{clear} \quad (1)$$

$$109 \quad LW_{cre} = LW_{total} - LW_{clear} \quad (2)$$

$$110 \quad NET_{cre} = SW_{cre} + LW_{cre} \quad (3)$$

111

112 **2.3 Earth's surface radiative budget:** Surface radiative fluxes are taken from the CERES SFC
113 EBAF Ed4.0 data set (Kato et al., 2018). The net SW and LW fluxes at the surface (SW_{sfc} and
114 LW_{sfc} , respectively) are calculated as the difference between the downwelling SW_{down} (LW_{down})
115 and upwelling SW_{up} (LW_{up}) as shown in equations 4 (5).

$$116 \quad SW_{sfc} = SW_{down} - SW_{up} \quad (4)$$

$$117 \quad LW_{sfc} = LW_{down} - LW_{up} \quad (5)$$

118 $NET_{sfc} = SW_{sfc} + LW_{sfc}$ (6)

119 **2.4 Sea ice concentration:** Sea ice concentration (SIC) data are from the National Snow and Ice
 120 Data Center (NSIDC, <http://nsidc.org/data/G02202>). This data set is a Climate Data Record (CDR)
 121 of SIC from passive microwave data and provides a consistent, daily and monthly time series of
 122 SIC from 09 July 1987 through the most recent processing for both the North and South Polar
 123 regions (Peng et al., 2013; W. Meier, F. Fetterer, M. Savoie, S. Mallory, R. Duerr, 2017). The data
 124 is provided on a 25 km x 25 km grid. We used the latest version (Version 3) of the SIC CDR
 125 created with a new version of the input product, from Nimbus-7 SMMR and DMSP SSM/I-SSMIS
 126 Passive Microwave Data.

127 **2.5 Polar seas:** We define the polar seas as ocean regions where the monthly SIC is larger than
 128 10% at least one month during 2001-2016 period. Polar seas extent is shown in Figure S1.

129 **2.6 CMIP5 Models** To reconstruct the historical CRE and surface energy budget and project their
 130 future changes, we used an ensemble of simulations conducted with 32 climate models (models
 131 used are shown in Figure 3 and S3) contributing to the Coupled Model Intercomparison Project
 132 Phase 5 (CMIP5) (Taylor et al., 2012). These model experiments provided: historical runs (1850-
 133 2005) in which all external forcings are consistent with observations and future runs (2006-2100)
 134 using the RCP8.5 emission scenarios (Taylor et al., 2012). The comparison with the satellite data
 135 is made over 2001-2016 by merging historical runs 2001-2005 with RCP8.5 2006-2016.

136 **2.7 Estimation of the local variations in radiative flux, cloud cover, and cloud optical depth**
 137 **concurrent with changes in sea ice concentration**

138 This study employs a novel method for quantifying the variations in radiative fluxes and cloud
 139 properties with SIC. This methodology leverages inter-annual variability of sea ice cover to assess
 140 these relationships. Figure 2 schematically shows the methodology based on the following steps.
 141 We use SW as an example and apply the approach in the same way to other variables.

142 1) ΔSW_j values are summarized in a schematized plot (Figure 2a) where each cell j in such plot
 143 shows the average ΔSW_m observed for all possible combinations of SIC at a grid box between two
 144 consecutive observation years (year y_i and y_{i+1} from time period 2001-2016) displayed on the X
 145 and Y axes, respectively. For the sake of clarity in Figure 2 the X and Y axes report SIC in intervals
 146 of 10%, while in Figure 5, 6, 7, S5 and S6 the axes are discretized with 2% bins.

147 2) Because of the regular latitude/longitude grid used in the analysis, the area of the grid cells (a_m)
 148 varies with the latitude. The energy signal (ΔSW_j) is therefore computed as an area weighted
 149 average (Equation 7) where M is the number of grid cells that are used to compute cell j in the
 150 schematised plot Fig 2a. Figure 2b shows the total area of all these grid cells as described by
 151 Equation 8.

152
$$\Delta SW_j = \frac{\sum_{m=1}^M a_m \Delta SW_m}{\sum_{m=1}^M a_m} \quad (7)$$

153 $A_j = \sum_{m=1}^M a_m$ (8)

154

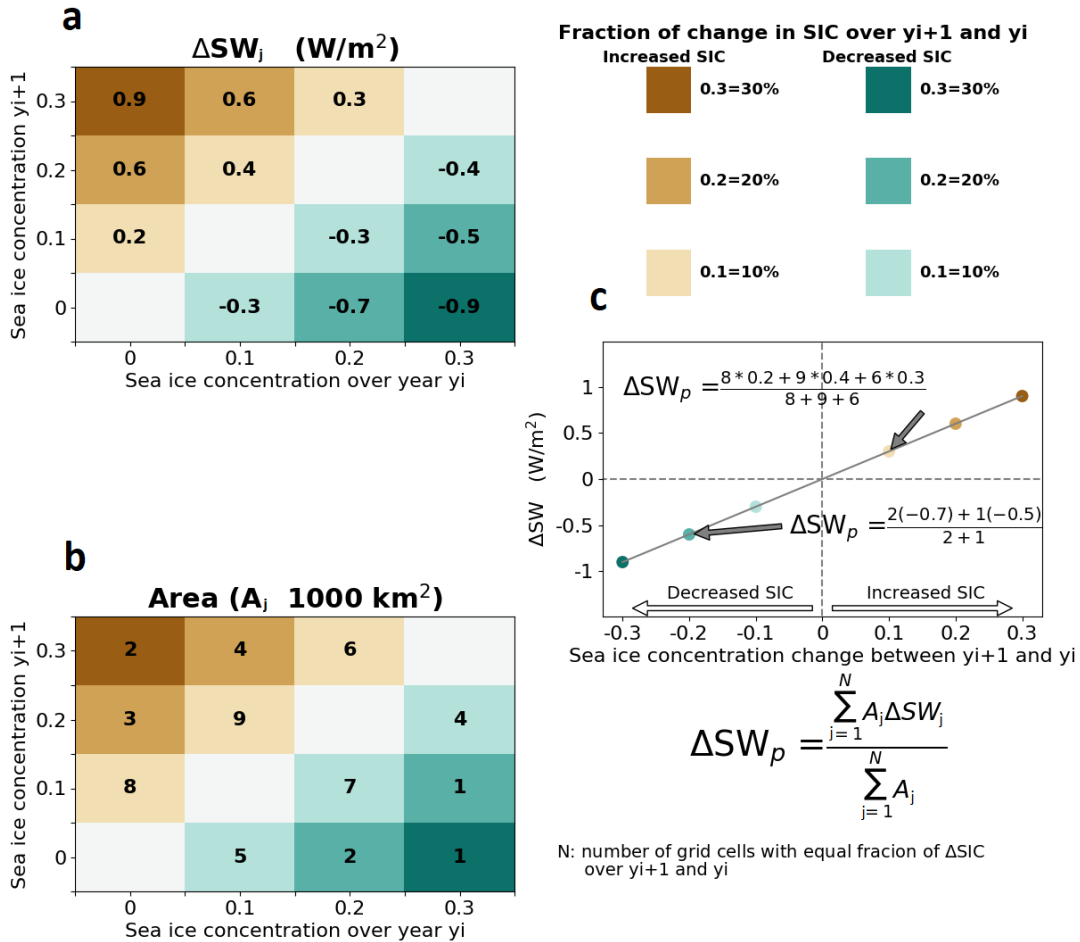
155 3) Calculation of the area weighted average (ΔSW_p) of the energy signal of all N cells with the
 156 same fraction X of a change in SIC (shown with the same colour in Figure 2a) Equation 9.

157
$$\Delta SW_p = \frac{\sum_{j=1}^N A_j \Delta SW_j}{\sum_{j=1}^N A_j}$$
 (9)

158 $\sum_{j=1}^N A_j$ is the total area of all grid cells with a particular SIC change.

159 ΔSW_p is the energy weighted average of all grid cells with a particular SIC change.

160



161

162 **Figure 2** Schematic representation of the methodology used to quantify the energy flux sensitivity
 163 to changes in sea ice concentration as a linear regression between the percentage of sea ice
 164 concentration and the variation in energy flux (right panel) using SW energy flux data and sea ice
 165 concentration defined in the left panels.

166

167 The average energy signals (ΔSW_p) per class of sea ice concentration change are reported in a
 168 scatterplot (Fig. 2 right panel) and used to estimate a regression line with zero intercept.

169 The slope S of this linear regression represents the local SW energy signal generated by the
 170 complete sea ice melting of a 1° grid cell. The weighted root mean square error (WRMSE) of the
 171 slope is estimated by Equation 10, where p represents one of the NP points in the scatterplot (Fig.
 172 2 right panel) and X_p is the relative change in sea ice concentration in the range ± 1 (equivalent to
 173 $\pm 100\%$ of sea ice cover change).

$$174 \quad WRMSE = \sqrt{\frac{\sum_{p=1}^{NP} A_p (\Delta SW_p - S X_p)^2}{\sum_{p=1}^{NP} A_p}}, \quad \text{where } A_p = \sum_{j=1}^N A_j \quad (10)$$

175 **2.8 Diagnosis of contributions to SWcre**

176 SWcre at the surface for the year y_i (Eq. 11) and year y_{i+1} (Eq. 12) is function of surface albedo
 177 α , SWdown under clear sky conditions ($SW \downarrow_{clr}$) and SWdown under total sky conditions
 178 ($SW \downarrow_{tot}$).

$$179 \quad SWcre_{y_i} = (1 - \alpha_{y_i})(SW \downarrow_{tot,y_i} - SW \downarrow_{clr,y_i}) \quad (11)$$

$$180 \quad SWcre_{y_{i+1}} = (1 - \alpha_{y_{i+1}})(SW \downarrow_{tot,y_{i+1}} - SW \downarrow_{clr,y_{i+1}}) \quad (12)$$

181

182 Using the first-order Taylor series expansion to (11) yields

$$183 \quad \Delta SWcre_{y_{i+1}-y_i} =$$

$$184 \quad (-\Delta \alpha_{y_{i+1}-y_i})(SW \downarrow_{tot,y_i} - SW \downarrow_{clr,y_i}) + (1 - \alpha_{y_i}) \Delta_{y_{i+1}-y_i} (SW \downarrow_{tot} - SW \downarrow_{clr}) \quad (13)$$

185

186 Where

$$187 \quad \Delta_{y_{i+1}-y_i} (SW \downarrow_{tot} - SW \downarrow_{clr}) = (SW \downarrow_{tot,y_{i+1}} - SW \downarrow_{clr,y_{i+1}}) - (SW \downarrow_{tot,y_i} - SW \downarrow_{clr,y_i}) \quad (14)$$

188

189 Separating the terms yields,

$$190 \quad \Delta SWcre_{ALB} = (-\Delta \alpha_{y_{i+1}-y_i})(SW \downarrow_{tot,y_i} - SW \downarrow_{clr,y_i}) \quad (15)$$

191 Where $\Delta SWcre_{ALB}$ is the part of SWcre change that is induced by the change in surface albedo.

192

$$193 \quad \Delta SWcre_{cloud} = (1 - \alpha_{y_i}) \Delta_{y_{i+1}-y_i} (SW \downarrow_{tot} - SW \downarrow_{clr}) \quad (16)$$

194 Where $\Delta SWcre_{cloud}$ is the part of SWcre change that is induced by the change in cloud cover and cloud
 195 optical depth.

196 $\Delta SWcre_{y_{i+1}-y_i} = \Delta SWcre_{ALB} + \Delta SWcre_{cloud}(17).$

197 The above equations are used in figure 7 and S5.

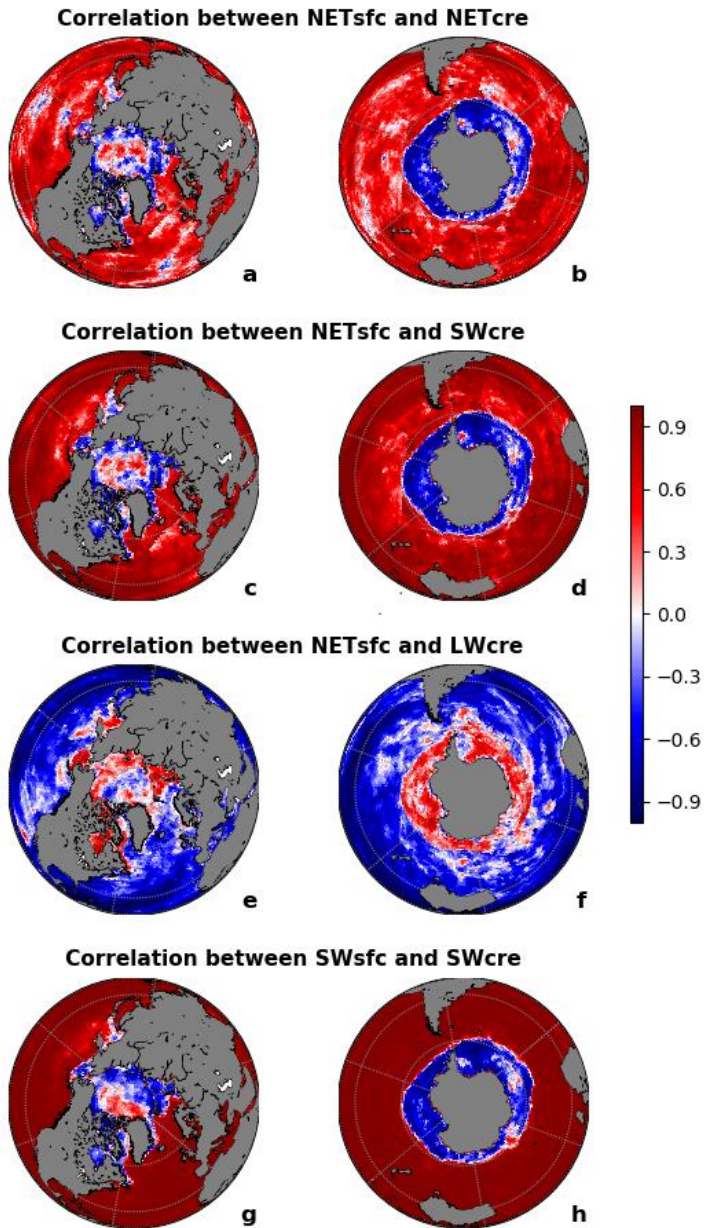
198

199 **3. Results and discussions**

200 **3.1 Negative correlation patterns between cloud radiative effect and surface radiation on** 201 **polar seas**

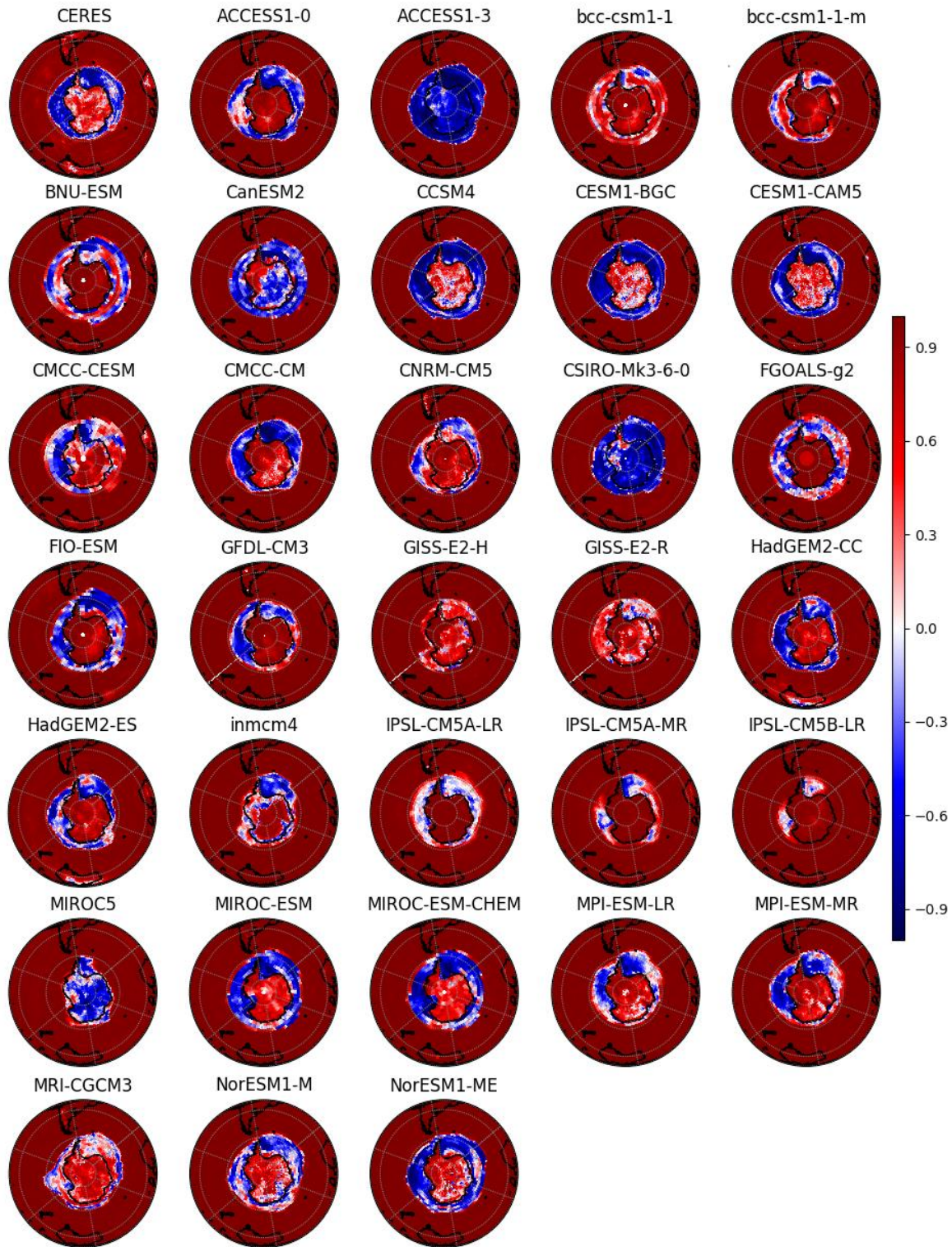
202

203 Given the known cloud influence on the surface radiative budget, a positive correlation between
204 TOA CRE and surface radiative budget is expected (the amount of absorbed radiation at the surface
205 decreases with a more negative SWcre and a less positive LWcre). Figure 3 illustrates a positive
206 correlation between the annual mean NETcre and NETsfc over much of the global ocean using the
207 CERES TOA flux data from 2001-2016. However, our analysis reveals the opposite pattern over
208 the polar seas (defined in section 2.5) where the correlation is negative over the Antarctic and
209 partly negative over the Arctic (Bering Strait, Hudson Bay, Barents Sea and the Canadian
210 Archipelago; Fig. 3ab). Considering the SWcre and LWcre components, we find that the SWcre
211 (Fig. 3cd) shows a similar pattern of correlation as the NETcre (Fig. 3ab) but with a stronger
212 magnitude, while LWcre generally shows the opposite correlations (Fig. 3ef). This suggests that
213 the factors influencing SWcre are responsible for the sharp contrast in the correlation found in the
214 polar regions. Indeed, SWsfc and SWcre (Fig. 3gh) show the sharpest and most significant contrast
215 between the polar regions and the rest of the world (Fig. S2 is similar to Fig. 3 but only significant
216 correlations at the 95% confidence level are reported in blue and red colors). Overall, climate
217 models are able to reproduce the spatial pattern of the observed SW correlation, but also show a
218 large inter-model spread in the spatial extent of the phenomena (Fig. 4 and S3). On the other hand,
219 several models completely fail to reproduce the correlation. ACCESS1-3, MIROC5, CanESM2
220 and CSIRO-Mk3-6-0 models show negative correlation over Antarctic continent in contrast to
221 observed positive correlation. Some models, like IPSL-CM5B-LR, GISS-E2-R and bcc-csm1-1,
222 fail to reproduce the observed negative correlation over the Southern Ocean. This suggests that
223 these models contain misrepresentations of the relationships SWcre and NETsfc likely resulting
224 from errors in the relationships between sea ice, surface albedo, cloud cover/thickness, and their
225 influence on surface radiative fluxes that could severely impact their projections. Moreover, Fig.
226 4 demonstrates that simple correlations between NETsfc and the individual radiation budget terms
227 represents a powerful metric for climate model evaluation allows for a quick check for realistic
228 surface radiation budget variability in polar regions.



229

230 **Figure 3** Correlation between TOA CRE and surface radiation budget terms over 2001-2016 from
 231 CERES measurements for the Northern Hemisphere (aceg) and Southern Hemisphere (bdfh) polar
 232 sea. Positive correlations shown by the red color indicate that years with less NETsfc coincide
 233 with years where NETcre has a stronger cooling effect and *vice versa*.



234

235 **Figure 4** Correlation between SWcre and SWsfc shown by 32 CMIP5 earth system models and
 236 CERES between 2001 and 2016 over the Southern Hemisphere.

237

238 3.2 Effects of sea ice concentration change

239
240 We illustrate that the apparent contradiction over the polar seas between NET_{cre} and NET_{sfc}
241 found in Fig 3ab is caused by the factors contributing to the SW fluxes. This can be explained by:
242 (I) SW_{cre} can change even if cloud properties are held constant due to the changes in clear-sky
243 radiation changes induced by changes in sea ice and surface albedo. When surface albedo is
244 reduced, the surface absorbs more sunlight at the surface resulting in a greater SW_{total}. At the
245 same time, SW_{clear} increases since the lower albedo allows a larger fraction of the extra
246 downwelling SW at the surface to be absorbed (see Fig. 1). Therefore, SW_{cre} becomes more
247 negative even in the absence of cloud changes (a purely surface-related effect); (II) On the other
248 hand, the relationship between cloud cover/thickness and sea ice could lead to cloudier Polar seas
249 under melting sea ice (Abe et al., 2016; Liu et al., 2012) such that the SW_{cre} decreases (increasing
250 the amount of SW reflected back to space by clouds, see Fig. 1), thus the cloud cooling effect is
251 enhanced concurrently with melting sea ice (a purely cloud-related effect). Both of these factors
252 occur simultaneously.

253
254 Over the Antarctic seas, analysis of the year-to-year changes in SW_{down} stratified in 2% SIC bins
255 retrieved from satellite microwave radiometer measurements (see section 2.7) shows an increase
256 in SW_{down} with increased SIC and *vice-versa* (Fig. 5a). This suggests that years with higher SIC
257 also have fewer and/or thinner clouds (Liu et al., 2012) (Fig. 6), larger SW_{down} and also larger
258 upward SW radiation (SW_{up}) (Fig. 5b), due to higher surface albedo (Fig. S4). Consequently,
259 these years show a more negative SW_{sfc} (Fig. 5c) and thus are characterized by stronger surface
260 cooling. Furthermore, fewer clouds implies a reduction of the cloud cooling effect (less negative
261 SW_{cre}) as described above in process (II), this accounts for $34 \pm 1\%$ (Fig. 7d) of the total change
262 in SW_{cre}, and as described in process (I) the increase in the surface albedo also makes SW_{cre} less
263 negative and explains $66 \pm 2\%$ of the observed change (Fig. 7d). Thus, the observed negative
264 correlation between SW_{cre} and SW_{sfc} over the polar seas results from the larger effects of process
265 (I) than (II). Similar results are found over the Arctic Ocean with slightly different sensitivity (Fig.
266 S5, S6). This difference is tied to differences in sun angle/available sunlight, as Antarctic sea ice
267 is concentrated at lower latitudes than Arctic sea ice.

268
269 Using the regression relationships derived from our composite analysis, we estimate the magnitude
270 of the cloud effect. For the Antarctic system, we use the numbers found in Figure 5e where we
271 find the annual mean relationship between NET_{sfc} (in W/m²) and SIC (fraction between 0 and 1),
272 and NET_{cre} (in W/m²) and SIC (fraction between 0 and 1).

$$273 \Delta \text{NET}_{\text{sfc}} = (-36.61 \pm 0.72) \Delta \text{SIC} \quad (18)$$

$$274 \Delta \text{NET}_{\text{cre}} = (47.03 \pm 1.01) \Delta \text{SIC} \quad (19)$$

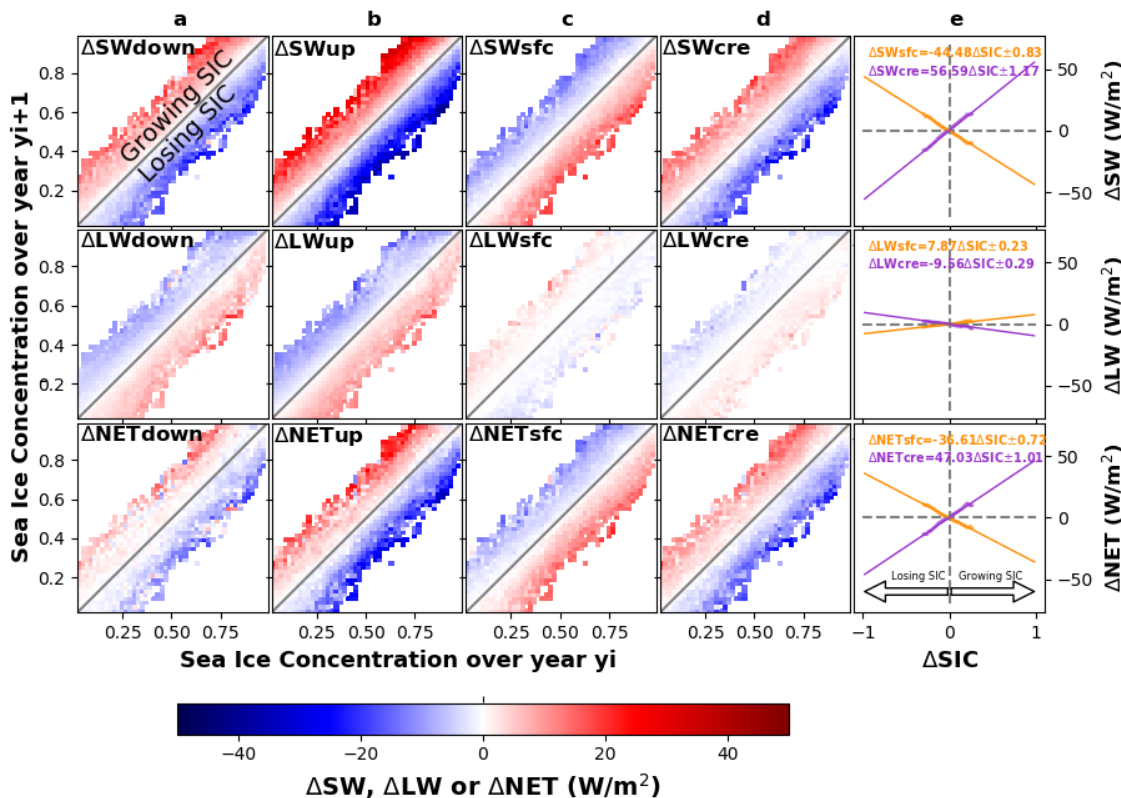
275
276 When excluding the CRE, the $\Delta \text{NET}_{\text{sfc}}$ would be equal to $(-36.61 - 47.03) \Delta \text{SIC} = -83.64 \Delta \text{SIC}$.

277 We estimate that the existence of clouds and their property variations are damping the potential
278 increase in the NET_{sfc} within the Antarctic system due to the surface albedo decrease from sea ice
279 melt by 56% ($47.03/83.64$). The uncertainty is calculated by summing the uncertainties shown in

280 equation (18) and (19) as follows: $(0.72^2+1.01^2)^{1/2}/83.64=2\%$.

281 Similarly, over the Arctic (Fig. S5), we compute the cloud influence on the surface net radiative
 282 budget that covaries with sea ice loss is $47\pm 3\%$, in agreement with the study of Sledd and L'Ecuyer
 283 (2019).

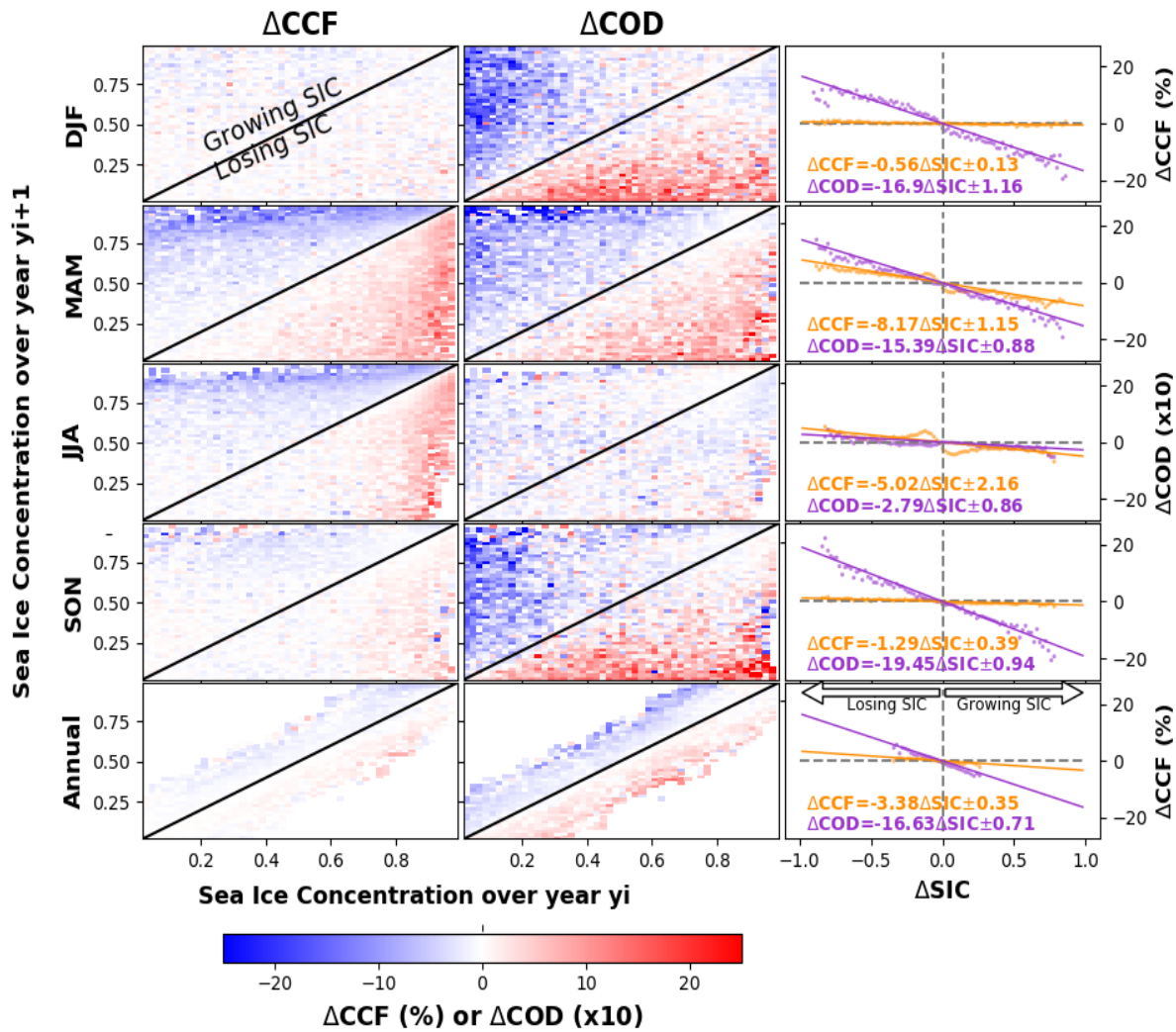
284



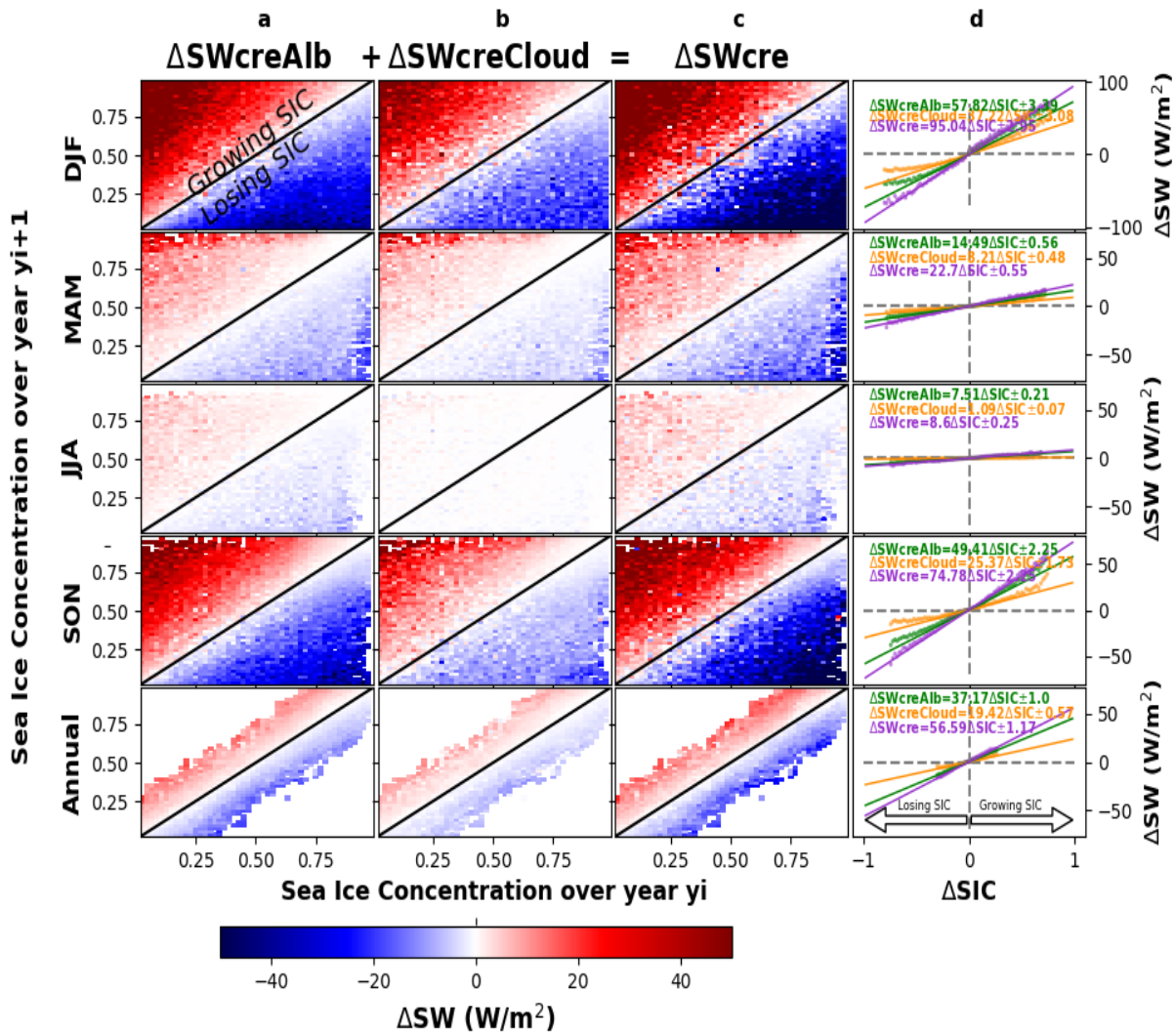
285 **Figure 5** Annual changes in SW, LW and NET as function of SIC. Annual changes in SW (top),
 286 LW (middle) and NET (bottom) of radiative down (a), up (b), sfc=down-up (c) and cre (d) over
 287 Antarctic sea as function of SIC change between two consecutive years y_{i+1} and y_i from 2001-2016
 288 time period. The top triangles in (c top) refers to the increase (growing) in SIC while the blue color
 289 means a reduction (cooling) in SWsfc. Whereas, the top triangles in (d) refers to the increase in
 290 SIC while the red color means an increase (decreasing the cooling role of clouds) in SWcre. Each
 291 dot in column (e) represents the average of one parallel to the diagonal in (c) or (d) as described in
 292 the Section 2.7.

293

294



295
 296 **Figure 6** Seasonal and annual changes in cloud cover fraction (CCF) and cloud optical depth
 297 (COD) over the Antarctic polar sea region as a function of SIC change between two consecutive
 298 years y_{i+1} and y_i from 2001-2016 time period. In order to use the same scale, COD has been
 299 multiplied by a factor 10. The top triangles in the two first columns refer to the increase (growing)
 300 in SIC while the blue color means a reduction in CCF or COD.
 301



302

303 **Figure 7** Seasonal and annual changes in SW_{creAlb} , $SW_{creCloud}$ and SW_{cre} over the Antarctic
 304 polar sea region as function of SIC change between two consecutive years y_{i+1} and y_i from 2001-
 305 2016 time period. The analysis is based on method described in section 2.7 and observations from
 306 satellites data.

307

308

309

310

311

312

313

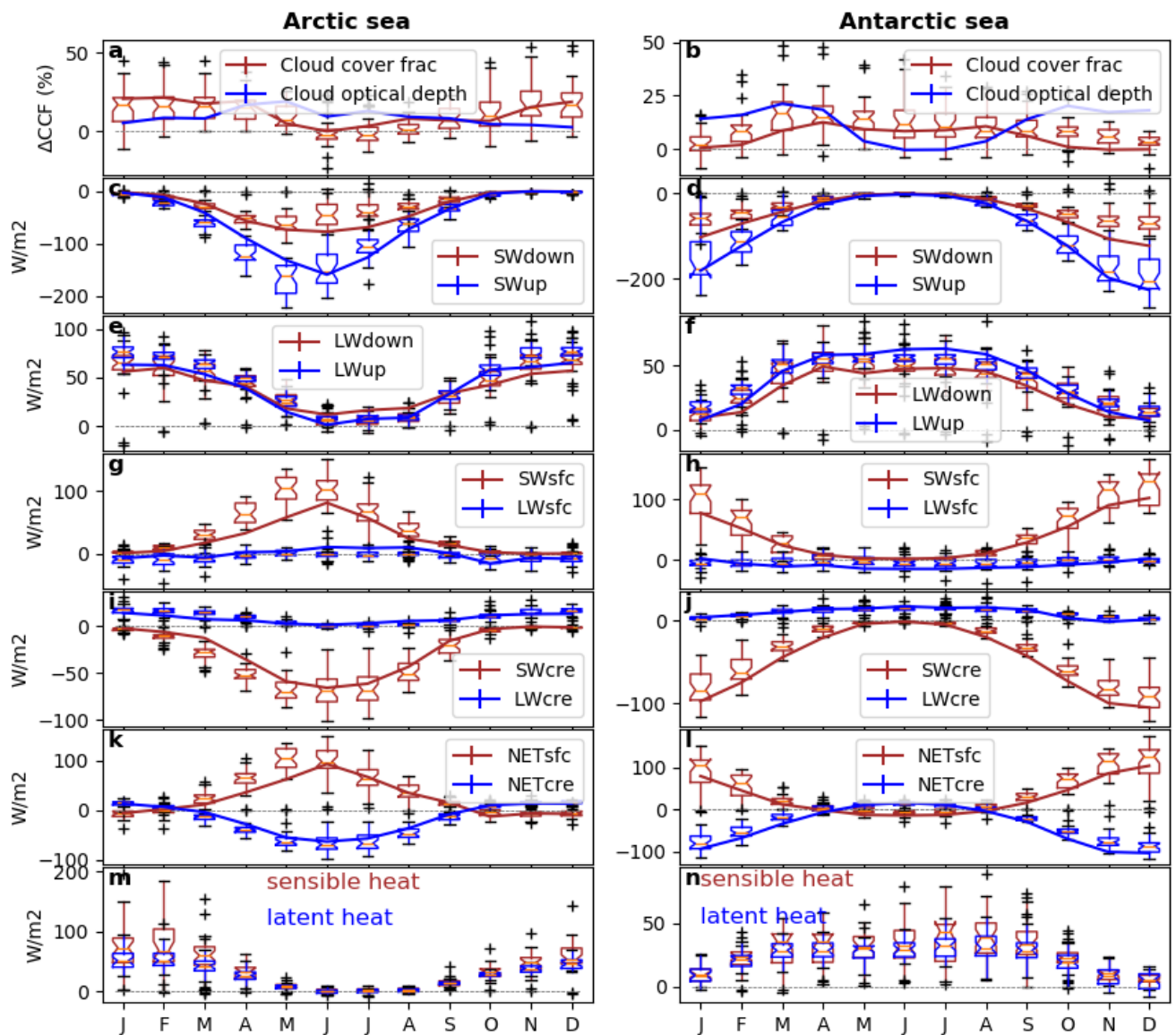
314 Altogether the results suggest clouds substantially reduce the impact of sea ice loss on the surface
315 radiation budget and thus the observed sea ice albedo feedback. This effect in the polar
316 climate system leads to a substantial reduction ($56\pm 2\%$ over the Antarctic and $47\pm 3\%$ over the
317 Arctic) of the potential increase in NETsfc in response to sea ice loss. This magnitude is similar to
318 a previous study (Qu and Hall 2006) showing across a climate model ensemble that clouds damped
319 the TOA effect of land surface albedo variations by half. Sledd and L'Ecuyer (2019) also
320 determined that the cloud damping effect (also referred to as cloud masking) of the TOA albedo
321 variability results from Arctic sea ice changes was approximately half. Despite this mechanism,
322 the sharp reduction in Arctic surface albedo has dominated the recent change in the surface
323 radiative budget and has led to a significant increase in NETsfc since 2001 in the CERES data
324 (Duncan et al. 2020). These results demonstrate that the trends in polar surface radiative fluxes are
325 driven by reductions in SIC and surface albedo and that clouds have partly mitigated the trend (i.e.,
326 a damping effect). Our findings highlight the importance of processes that control sea ice albedo
327 (i.e. sea ice dynamics, snowfall, melt pond formation, and the deposition of black carbon), as the
328 surface albedo of the polar seas in regions of seasonal sea ice is crucial for the climate dynamics.

329 **3.3 Sensitivity of the surface energy budget to variability of sea ice concentration**

330 Our results are consistent with other recent studies (Taylor et al., 2015; Morrison et al. 2018) that
331 demonstrate a CCF response to reduced sea ice in fall/winter but not in summer (Figure 8a) over
332 the Arctic Ocean. The lack of a summer cloud response to sea ice loss is explained by the prevailing
333 air-sea temperature gradient, where near surface air temperatures are frequently warmer than the
334 surface temperature (Kay and Gettelman 2009). Surface temperatures in regions of sea ice melt
335 hover near freezing due to the phase change, whereas the atmospheric temperatures are not
336 constrained by the freezing/melting point. Despite reduced sea ice cover, strong increases in
337 surface evaporation (latent heat) are limited (Fig. 8mn), as also suggested by the small trends in
338 surface evaporation rate derived from satellite-based estimates (Boisvert and Stroeve, 2015; Taylor
339 et al., 2018). We argue that the strong increase of SWcreCloud under decreased sea ice observed
340 during summer is induced by larger values of COD (Fig. 8a), which depend on the liquid or ice
341 water content. We also show that the relationships derived from our observation-driven analysis
342 match the projected changes in the Arctic and Antarctic surface energy budget in the median
343 CMIP5 model ensemble (Fig. 8). However, we find a large spread amongst climate models that
344 indicates considerable uncertainty.

345 Analyzing the seasonal cycle of the sensitivity of the surface energy budget to SIC variability, we
346 found that SWsfc (SWcre) explains most of the observed changes in the NETsfc (NETcre) during
347 summer, while LWsfc plays a minor role (Fig. 8). In contrast, during winter LWsfc (LWcre)
348 explains most of the observed changes in the NETsfc (NETcre). In general, the median of the 32
349 CMIP5 (Taylor et al., 2012) climate models captures the observed sensitivity of the radiative
350 energy budget and cloud cover change to SIC but the spread between climate models is large,
351 especially for CCF. We have to note here that, the numbers reported in Figure 8 are for 100% SIC
352 loss, while the ones reported in the previous figures (Fig. 5, 6 and 7) are for 100% SIC gain,
353 explaining the opposite sign.

354



356
 357
 358
 359
 360
 361
 362
 363
 364
 365
 366
 367
 368

Figure 8 Monthly change in different terms of the radiative energy balance, cloud optical depth (COD) and cloud cover fraction (CCF) extrapolated from observations for a hypothetical 100% decrease in SIC over the areas where SIC change was observed during the period 2001-2016. This estimate came from the use of a linear interpolation of the change of different parts of the energy budget, COD and CCF as function of a change in SIC coming from all possible combinations of couplets of consecutive years for a given month from 2001 to 2016 and for all grid cells for which SIC is larger than zero in one of the two years (see section 2.7). CERES data are shown by solid lines (the standard deviation of the slopes are also reported but are too small to be visible) while CMIP5 models are shown by boxplot and the box (are in same color as observations) represents the first and third quartiles (whiskers indicate the 99% confidence interval and black markers show outliers). In order to use the same scale, COD has been multiplied by a factor 10.

369

370 **3.4 Projections and uncertainties of cloud radiative effects on surface energy budget**

371 Under the RCP8.5 scenario (a business as usual case; Taylor et al., 2012), CMIP5 models show an
372 increase in SWsfc over the Arctic Ocean (Fig. 9a) consistent with the expected large decrease in
373 the SIC (Comiso et al., 2008; Serreze et al., 2007; Stroeve et al., 2007). This increase in SWsfc
374 occurs despite the relatively large, concurrent and opposing change in cloud cooling effect
375 (SWcre). Future LW fluxes (Fig. 9c) will likely play a smaller but non-negligible role on total
376 energy budget by further increasing NETsfc (Fig. 9e) and reducing NETcre. In addition, CMIP5
377 models show clearly that by 2100, the magnitude of the decrease in NETcre is slightly smaller than
378 the increase in NETsfc (Fig. 9e) over Arctic Ocean. While the Antarctic polar sea region shows
379 the opposite (Fig. 9f). This is in line with the estimated dampening effect of clouds coming from
380 CERES over 2001-2016 that is about $47\pm 3\%$ in the Arctic and $56\pm 2\%$ in the Antarctic. Indeed, the
381 stronger cloud damping effect in the Antarctic region cause the NETcre to become even more
382 negative than the Arctic (Fig. 9gh).

383

384 Large uncertainties remain in the decline rate of summer sea ice and the timing of the first
385 occurrence of a sea ice-free Arctic summer (Arzel et al., 2006; Zhang and Walsh, 2006). The
386 reason behind the large spread between climate models is still debated (Holland et al., 2017;
387 Simmonds, 2015; Turner et al., 2013). In this study, we explored the annual mean Arctic and
388 Antarctic sea-ice extent trend from 32 CMIP5 models and find a large positive correlation with
389 the simulated trend in the SWdown (Figure 9gh). This analysis suggests that the models showing
390 a larger trend in cloud cover also show larger decreases in sea-ice extent and suggest that a stronger
391 coupling of these two variables may occur in the future. However, the direction of causality
392 between the two variables is unclear. We also note that from the 32 models tested, only few show
393 consistent trends in both SWdown and SIC over 2001-2016 (Figure 9gh).

394

395 **4. Conclusion**

396 The manuscript addresses two important climate science topics, namely the role of clouds and the
397 fate of polar sea ice. The work is grounded in a long time series of robust satellite observations
398 that allowed us to document an important damping effect in the polar cloud-sea ice system using
399 a unique inter-annual approach. Our results agree with several previous works that approached the
400 problem from a different perspective (Hartmann and Ceppi 2014; Sledd and L'Ecuyer 2019). In
401 addition, we show how 32 state-of-the-art climate models represent aspects of the surface radiation
402 budget over the polar seas.

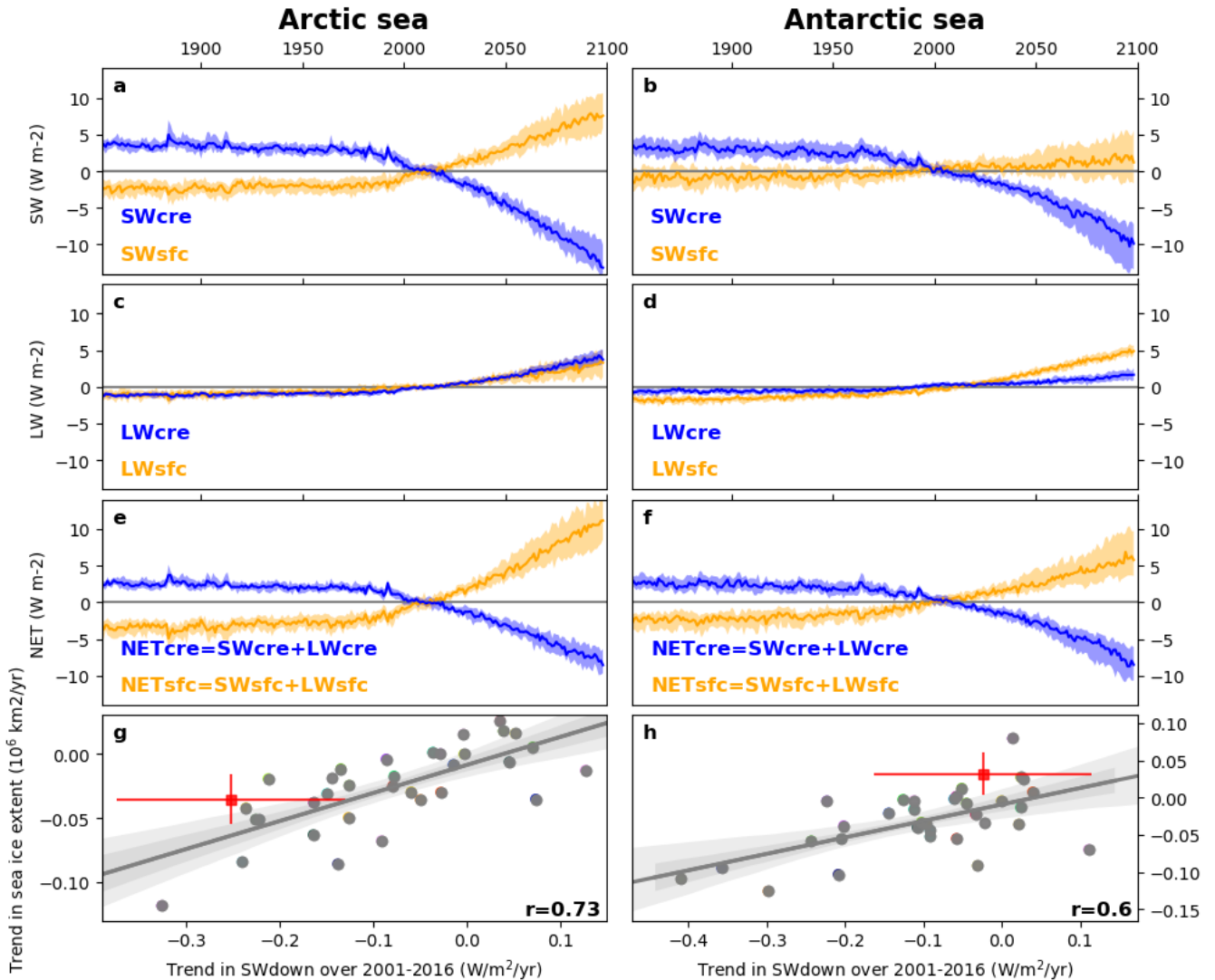
403

404 Our data-driven analysis shows that polar sea-ice and clouds interplay in a way that substantially
405 reduces the impact of the sea ice loss on the surface radiation budget. We found that when sea ice
406 cover is reduced between two consecutive years that the cloud radiative effect becomes more
407 negative, damping the total change in the net surface energy budget. The magnitude of this effect

408 is important. Satellite data indicates that the more negative cloud radiative effect reduces the
409 potential increase of net radiation at the surface by approximately half. One-third of this cloud
410 radiative effect change is induced by the direct change in cloud cover/thickness, while two-thirds
411 of this change results from the surface albedo change.
412

413 In addition, we demonstrated that the models that show larger trends in polar sea ice extent also
414 show larger trends in surface net solar radiation. In order to understand current and future climate
415 trajectories, model developments should aim at reducing uncertainties in the representation of
416 polar cloud processes in order to improve the simulation of present-day cloud properties over the
417 polar seas. Present-day Arctic and Antarctic cloud properties strongly influence the model
418 simulated cloud damping effect on the radiative impacts of sea ice loss.
419

420 Future cloud changes and sea ice evolution represent major uncertainties in climate projections
421 due to the multiple relevant pathways through which cloudiness and sea ice feed back on Earth's
422 climate system (Solomon, S., D. Qin, M. Manning, Z. Chen, M. Marquis, K.B. Averyt, 2007). Our
423 evidence derived from Earth observations provides additional insight into the coupled radiative
424 impacts of polar clouds and the changing sea ice cover (Fig. 8) that may provide a useful constraint
425 on model projections and ultimately improve our understanding of present and future polar
426 climate. At the very least, our results demonstrate a simple correlation analysis between the net
427 surface radiation budget and individual radiation budget terms that can be used to quickly evaluate
428 climate models for realistic surface radiation budget variability in polar regions. Ultimately, our
429 findings on the interplay between cloud and sea ice may support an improvement in the model
430 representation of the cloud-ice interactions, mechanisms that may substantially affect the speed of
431 the polar sea ice retreat, which in turn has a broad impact on the climate system, on the Arctic
432 environment and on potential economic activities in the Arctic region (Buixadé Farré et al., 2014).



433

434 **Figure 9** Time series of the anomaly in respect to the whole period 1850-2100 of the radiative
 435 flux. Mean modeled SWcre, LWcre and NETcre (blue) and surface SWsfc, LWsfc and NETsfc
 436 (orange) anomalies over the 1850-2100 period under rcp8.5 scenario averaged over the Arctic sea.
 437 The solid line shows the median, where the envelope represents the 25 and 75 percentile of the 32
 438 CMIP5 models. The linear regression (grey solid line and its 68% (dark grey envelope) and 95%
 439 (light grey envelope) confidence interval) between: the trend in SWdown and trend in sea ice
 440 extent (g and h); of the 32 CMIP5 climate models shown by grey dots over 2001-2016. The
 441 observed trends are shown by red colors where confidence interval refers to standard error of the
 442 trend.

443

444

445

446

447 **Acknowledgments:** The authors acknowledge the use of Clouds and the Earth's Radiant Energy
448 System (CERES) satellite data version 4.0 from <https://ceres.larc.nasa.gov/index.php>, sea ice
449 concentration data from National Snow and Ice Data Center (NSIDC) <http://nsidc.org/data/G02202>, as
450 well as the modeling groups that contributed to the CMIP5 data archive at PCMDI
451 <https://cmip.llnl.gov/cmip5/>.

452

453 **Author Contributions:** RA designed the study and performed the analysis. RA, AC, PCT and LGS
454 contributed to the interpretation of the results. RA, PCT, AC and GD drafted the paper. All authors
455 commented on the text.

456 **Competing interests:** The authors declare no competing financial interests.

457 **Additional information:** The programs used to generate all the results are made with Python.
458 Analysis scripts are available by request to R. Alkama.

459 **References:**

460

461 Abe, M., Nozawa, T., Ogura, T. and Takata, K.: Effect of retreating sea ice on Arctic cloud cover
462 in simulated recent global warming, *Atmos. Chem. Phys.*, 16, 14343–14356, doi:10.5194/acp-16-
463 14343-2016, 2016.

464

465 Arzel, O., Fichefet, T. and Goosse, H.: Sea ice evolution over the 20th and 21st centuries as
466 simulated by current AOGCMs, *Ocean Model.*, 12(3-4), 401–415,
467 doi:10.1016/J.OCEMOD.2005.08.002, 2006.

468

469 Boeke, R. C. and P. C. Taylor: Evaluation of the Arctic surface radiation budget in CMIP5
470 models. *J. Geophys. Res.*, **121**, 8525-8548, doi: 10.1002/2016JD025099, 2016.

471

472 Boisvert, L. N. and Stroeve, J. C.: The Arctic is becoming warmer and wetter as revealed by the
473 Atmospheric Infrared Sounder, *Geophys. Res. Lett.*, 42(11), 4439–4446,
474 doi:10.1002/2015GL063775, 2015.

475

476 Buixadé Farré, A., Stephenson, S. R., Chen, L., Czub, M., Dai, Y., Demchev, D., Efimov, Y.,
477 Graczyk, P., Grythe, H., Keil, K., Kivekäs, N., Kumar, N., Liu, N., Matelenok, I., Myksovoll, M.,
478 O’Leary, D., Olsen, J., Pavithran.A.P., S., Petersen, E., Raspotnik, A., Ryzhov, I., Solski, J., Suo,
479 L., Troein, C., Valeeva, V., van Rijckevorsel, J. and Wighting, J.: Commercial Arctic shipping
480 through the Northeast Passage: routes, resources, governance, technology, and infrastructure,
481 *Polar Geogr.*, 37(4), 298–324, doi:10.1080/1088937X.2014.965769, 2014.

482

483 Cesana, G., J. E. Kay, H. Chepfer, J. M. English, and G. de Boer: Ubiquitous low-level liquid-
484 containing Arctic clouds: New observations and climate model constraints from CALIPSO-
485 GOCCP, *Geophys. Res. Lett.*, 39, L20804, doi:10.1029/2012GL053385. 2012.

486
487 Charlock, T. P. and Ramanathan, V.: The Albedo Field and Cloud Radiative Forcing Produced
488 by a General Circulation Model with Internally Generated Cloud Optics, *J. Atmos. Sci.*, 42(13),
489 1408–1429, doi:10.1175/1520-0469(1985)042<1408:TAFACR>2.0.CO;2, 1985.
490
491 Cheung, W. W. L., Lam, V. W. Y., Sarmiento, J. L., Kearney, K., Watson, R. and Pauly, D.:
492 Projecting global marine biodiversity impacts under climate change scenarios, *Fish Fish.*, 10(3),
493 235–251, doi:10.1111/j.1467-2979.2008.00315.x, 2009.
494
495 Christensen, M., A. Behrangi, T. L'Ecuyer, N. Wood, M. Lebsock, and G. Stephens: Arctic
496 observation and reanalysis integrated system: A new data product for validation and climate study,
497 *Bull. Am. Meteorol. Soc.*, doi:10.1175/BAMS-D-14-00273.1, 2016.

498
499 Cohen, J., Screen, J. A., Furtado, J. C., Barlow, M., Whittleston, D., Coumou, D., Francis, J.,
500 Dethloff, K., Entekhabi, D., Overland, J. and Jones, J.: Recent Arctic amplification and extreme
501 mid-latitude weather, *Nat. Geosci.*, 7(9), 627–637, doi:10.1038/ngeo2234, 2014.
502
503 Cohen, J., Zhang, X., Francis, J. *et al.* Divergent consensuses on Arctic amplification influence
504 on midlatitude severe winter weather. *Nat. Clim. Chang.* **10**, 20–29 (2020).
505 <https://doi.org/10.1038/s41558-019-0662-y>, 2019.

506
507 Comiso, J. C., Parkinson, C. L., Gersten, R., Stock, L.: Accelerated decline in the arctic sea ice
508 cover, *Geophys. Res. Lett.* <http://citeseerx.ist.psu.edu/viewdoc/summary?doi=10.1.1.419.8464>,
509 2008.
510
511 Curry, J. A., Schramm, J. L., Rossow, W. B. and Randall, D.: Overview of Arctic Cloud and
512 Radiation Characteristics, *J. Climate*, 9(8), 1731–1764, doi:10.1175/1520-
513 0442(1996)009<1731:OOACAR>2.0.CO;2, 1996.
514
515 Duncan, B. N., Ott, L. E., Abshire, J. B., Brucker, L., Carroll, M. L., Carton, J. and
516 coauthors: Space-based observations for understanding changes in the arctic-boreal
517 zone. *Reviews of Geophysics*, 58, e2019RG000652. <https://doi.org/10.1029/2019RG000652>,
518 2020.
519
520 Graverson, R. G., Mauritsen, T., Tjernström, M., Källén, E. and Svensson, G.: Vertical structure
521 of recent Arctic warming, *Nature*, 451(7174), 53–56, doi:10.1038/nature06502, 2008.
522
523 Harrison, E. F., Minnis, P., Barkstrom, B. R., Ramanathan, V., Cess, R. D. and Gibson, G. G.:
524 Seasonal variation of cloud radiative forcing derived from the Earth Radiation Budget
525 Experiment, *J. Geophys. Res.*, 95(D11), 18687, doi:10.1029/JD095iD11p18687, 1990.
526
527 Holland, M. M., Landrum, L., Raphael, M. and Stammerjohn, S.: Springtime winds drive Ross
528 Sea ice variability and change in the following autumn, *Nat. Commun.*, 8(1), 731,
529 doi:10.1038/s41467-017-00820-0, 2017.
530

531 Kato, E., Kinoshita, T., Ito, A., Kawamiya, M. and Yamagata, Y.: Evaluation of spatially explicit
532 emission scenario of land-use change and biomass burning using a process-based
533 biogeochemical model, *J. Land Use Sci.*, 8(1), 104–122, doi:10.1080/1747423X.2011.628705,
534 2013.

535

536 Kay, J. E., and Gettelman, A. : Cloud influence on and response to seasonal Arctic sea ice loss, *J.*
537 *Geophys. Res.*, 114, D18204, doi:10.1029/2009JD011773, 2009.

538

539 Kay, J. E., and T. L'Ecuyer: Observational constraints on Arctic Ocean clouds and radiative
540 fluxes during the early 21st century, *J. Geophys. Res. Atmos.*, 118, 7219–7236,
541 doi:10.1002/jgrd.50489, 2013.

542

543 Kay, J. E., T. L'Ecuyer, H. Chepfer, N. Loeb, A. Morrison, and G. Cesana: Recent advances in
544 Arctic cloud and climate research, *Curr. Clim. Change Rep.*, 2, 159, doi:10.1007/s40641-016-
545 0051-9. 2016.

546

547 Komurcu, M., T. Storelvmo, I. Tan, U. Lohmann, Y. Yun, J. E. Penner, Y. Wang, X. Liu, and T.
548 Takemura: Intercomparison of the cloud water phase among global climate models, *J. Geophys.*
549 *Res. Atmos.*, 119, 3372– 3400, doi:10.1002/2013JD021119. 2014.

550

551 Liu, Y., Key, J. R., Liu, Z., Wang, X. and Vavrus, S. J.: A cloudier Arctic expected with
552 diminishing sea ice, *Geophys. Res. Lett.*, 39(5), doi:10.1029/2012GL051251, 2012.

553

554 Loeb, N. G., Doelling, D. R., Wang, H., Su, W., Nguyen, C., Corbett, J. G., Liang, L., Mitrescu,
555 C., Rose, F. G., Kato, S., Loeb, N. G., Doelling, D. R., Wang, H., Su, W., Nguyen, C., Corbett, J.
556 G., Liang, L., Mitrescu, C., Rose, F. G. and Kato, S.: Clouds and the Earth's Radiant Energy
557 System (CERES) Energy Balanced and Filled (EBAF) Top-of-Atmosphere (TOA) Edition-4.0
558 Data Product, *J. Clim.*, 31(2), 895–918, doi:10.1175/JCLI-D-17-0208.1, 2018.

559

560 Loeb, N.G., H. Wang, F.G. Rose, S. Kato, W.L. Smith, and S. Sun-Mack: Decomposing
561 Shortwave Top-of-Atmosphere and Surface Radiative Flux Variations in Terms of Surface and
562 Atmospheric Contributions. *J. Climate*, **32**, 5003–5019, [https://doi.org/10.1175/JCLI-D-18-](https://doi.org/10.1175/JCLI-D-18-0826.1)
563 0826.1, 2019.

564

564 Morrison, A. L., Kay, J. E., Chepfer, H., Guzman, R. and Yettella, V.: Isolating the Liquid Cloud
565 Response to Recent Arctic Sea Ice Variability Using Spaceborne Lidar Observations, *Journal of*
566 *Geophysical Research: Atmospheres*, 123(1), 473–490, doi:10.1002/2017JD027248, 2018.

567

568 Peng, G., Meier, W. N., Scott, D. J. and Savoie, M. H.: A long-term and reproducible passive
569 microwave sea ice concentration data record for climate studies and monitoring, *Earth Syst. Sci.*
570 *Data*, 5(2), 311–318, doi:10.5194/essd-5-311-2013, 2013.

571

572 Post, E., Bhatt, U. S., Bitz, C. M., Brodie, J. F., Fulton, T. L., Hebblewhite, M., Kerby, J., Kutz,
573 S. J., Stirling, I. and Walker, D. A.: Ecological consequences of sea-ice decline., *Science*,
574 341(6145), 519–24, doi:10.1126/science.1235225, 2013.

575
576 Qu, X. and A. Hall: Assessing snow albedo feedback in simulated climate change. *J.*
577 *Climate*,19(11), 2617–2630, 2006
578
579 Ramanathan, V., Cess, R. D., Harrison, E. F., Minnis, P., Barkstrom, B. R., Ahmad, E. and
580 Hartmann, D.: Cloud-radiative forcing and climate: results from the Earth radiation budget
581 experiment., *Science* (80-.), 243(4887), 57–63, doi:10.1126/science.243.4887.57, 1989.
582
583 Serreze, M. C., Holland, M. M. and Stroeve, J.: Perspectives on the Arctic’s Shrinking Sea-Ice
584 Cover, *Science* (80-.), 315(5818), 1533–1536, doi:10.1126/science.1139426, 2007.
585
586 Simmonds, I.: Comparing and contrasting the behaviour of Arctic and Antarctic sea ice over the
587 35 year period 1979-2013, *Ann. Glaciol.*, 56(69), 18–28, doi:10.3189/2015AoG69A909, 2015.
588
589 Sledd A. and L'Ecuyer T.: How Much Do Clouds Mask the Impacts of Arctic Sea Ice and Snow
590 Cover Variations? Different Perspectives from Observations and Reanalyses. *Atmosphere*,
591 10(1), 12; <https://doi.org/10.3390/atmos10010012>, 2019.
592
593 Solomon, S., D. Qin, M. Manning, Z. Chen, M. Marquis, K.B. Averyt, M. T. and H. L. M.:
594 Contribution of Working Group I to the Fourth Assessment Report of the Intergovernmental
595 Panel on Climate Change, 2007.
596 http://www.ipcc.ch/publications_and_data/ar4/wg1/en/contents.html, 2007.
597
598 Stroeve, J., Holland, M. M., Meier, W., Scambos, T. and Serreze, M.: Arctic sea ice decline:
599 Faster than forecast, *Geophys. Res. Lett.*, 34(9), doi:10.1029/2007GL029703, 2007.
600
601 Taylor, K. E., Stouffer, R. J. and Meehl, G. A.: An Overview of CMIP5 and the Experiment
602 Design, *Bull. Am. Meteorol. Soc.*, 93(4), 485–498, doi:10.1175/BAMS-D-11-00094.1, 2012.
603
604 Taylor, P., Hegyi, B., Boeke, R. and Boisvert, L.: On the Increasing Importance of Air-Sea
605 Exchanges in a Thawing Arctic: A Review, *Atmosphere* (Basel)., 9(2), 41,
606 doi:10.3390/atmos9020041, 2018.
607
608 Taylor, P. C., Kato, S., Xu, K.-M. and Cai, M.: Covariance between Arctic sea ice and clouds
609 within atmospheric state regimes at the satellite footprint level, *J. Geophys. Res. Atmos.*,
610 120(24), 12656–12678, doi:10.1002/2015JD023520, 2015.
611
612 Trepte Q. Z. et al., "Global Cloud Detection for CERES Edition 4 Using Terra and Aqua MODIS
613 Data," in *IEEE Transactions on Geoscience and Remote Sensing*, vol. 57, no. 11, pp. 9410-9449,
614 Nov. 2019.
615
616 Turner, J., Bracegirdle, T. J., Phillips, T., Marshall, G. J., Hosking, J. S., Turner, J., Bracegirdle,
617 T. J., Phillips, T., Marshall, G. J. and Hosking, J. S.: An Initial Assessment of Antarctic Sea Ice
618 Extent in the CMIP5 Models, *J. Clim.*, 26(5), 1473–1484, doi:10.1175/JCLI-D-12-00068.1,
619 2013.
620

621 Meier W., F. Fetterer, M. Savoie, S. Mallory, R. Duerr, and J. S.: NOAA/NSIDC Climate Data
622 Record of Passive Microwave Sea Ice Concentration, Version 3. Boulder, Colorado USA.
623 NSIDC: National Snow and Ice Data Center., , doi:<https://doi.org/10.7265/N59P2ZTG>, 2017.
624
625 Zhang, X. and Walsh, J. E.: Toward a Seasonally Ice-Covered Arctic Ocean: Scenarios from the
626 IPCC AR4 Model Simulations, J. Clim